

See discussions, stats, and author profiles for this publication at: <https://www.researchgate.net/publication/375639750>

Synthesis, spectrophotometric, pharmacology and theoretical investigation of a new electron transfer complex of 8-hydroxyquinoline with oxalic acid in different polar solvents

Article in *Journal of biomolecular Structure & Dynamics* · November 2023

DOI: 10.1080/07391102.2023.2279277

CITATIONS

0

READS

31

10 authors, including:



Syed Khalid Mustafa

University of Tabuk

80 PUBLICATIONS 400 CITATIONS

SEE PROFILE



Rasha Jame

University of Tabuk

16 PUBLICATIONS 46 CITATIONS

SEE PROFILE



Noha Omer

University of Tabuk

6 PUBLICATIONS 2 CITATIONS

SEE PROFILE

Synthesis, spectrophotometric, pharmacology and theoretical investigation of a new electron transfer complex of 8-hydroxyquinoline with oxalic acid in different polar solvents

Syed Khalid Mustafa, Rasha Jame, Meshari M. H. Aljohani, Noha Omer, Ali Hamzah Alessa, Menier Al-Anazi, Fatimah A. Alotaibi, Matiur Sk, Maidul Islam & Sonam Shakya

To cite this article: Syed Khalid Mustafa, Rasha Jame, Meshari M. H. Aljohani, Noha Omer, Ali Hamzah Alessa, Menier Al-Anazi, Fatimah A. Alotaibi, Matiur Sk, Maidul Islam & Sonam Shakya (14 Nov 2023): Synthesis, spectrophotometric, pharmacology and theoretical investigation of a new electron transfer complex of 8-hydroxyquinoline with oxalic acid in different polar solvents, Journal of Biomolecular Structure and Dynamics, DOI: [10.1080/07391102.2023.2279277](https://doi.org/10.1080/07391102.2023.2279277)

To link to this article: <https://doi.org/10.1080/07391102.2023.2279277>

 View supplementary material 

 Published online: 14 Nov 2023.

 Submit your article to this journal 

 Article views: 43

 View related articles 

 View Crossmark data 



Synthesis, spectrophotometric, pharmacology and theoretical investigation of a new electron transfer complex of 8-hydroxyquinoline with oxalic acid in different polar solvents

Syed Khalid Mustafa^a, Rasha Jame^a, Meshari M. H. Aljohani^a, Noha Omer^a, Ali Hamzah Alessa^a, Menier Al-Anazi^a, Fatimah A. Alotaibi^a, Matiur Sk^b, Maidul Islam^b and Sonam Shakya^b 

^aDepartment of Chemistry, Faculty of Science, University of Tabuk, Tabuk, Saudi Arabia; ^bDepartment of Chemistry, Faculty of Science, Aligarh Muslim University, Aligarh, India

Communicated by Ramaswamy H. Sarma

ABSTRACT

Preparation, characterization, and investigation of a novel organic charge transfer (CT) complex were carried out, with a focus on exploring its antibacterial and antifungal characteristics. Theoretical analysis backs up the experimental findings. CT complex formed was synthesized between 8-hydroxyquinoline (8HQ) and oxalic acid (OA) at RT (room temperature). Different analyses were used to describe the CT complex, including ¹H-NMR, FTIR, TGA/DTA, and UV-vis spectra (in different solvents). These indicate that the CT interaction is linked to proton transfer from OA to 8HQ and the subsequent development of 'N⁺—H...O⁻' type bonding. On the basis of wave number, the CT complex and reactants are distinguished in FTIR spectra. By using Thermo gravimetric Analysis/Differential Thermal Analysis (TGA/DTA) tests, the thermal stability of complicated and thorough corrosion was examined. Through UV-visible spectroscopy, physical characteristics like E_{CT} (interaction energy), R_N (resonance energy), I_D (ionization potential), f (oscillator strength) and ΔG (free energy) were calculated. The ε_{CT} (molar extinction coefficient), the K_{CT} (formation constant), and additional physical properties of this complex were calculated by the Benesi-Hildebrand equation in order to determine its 1:1 stoichiometry. The biological properties are also supported by theoretical study. The protein, Human Serum Albumin (HSA), is observed to bind with CT complex, as shown by molecular docking and the observed binding energy value is -167.04 kcal/mol. Molecular dynamics (MD) simulation 100 ns run was used to refine docking results and binding free energy was calculated using MM-PBSA. This study introduces a novel CT complex, offering fresh perspectives on molecular interactions.

Abbreviations: CT: charge transfer; HSA: human serum albumin; 8-HQ: 8-hydroxyquinoline; OA: oxalic acid; ¹H-NMR: hydrogen or proton NMR; FTIR: Fourier-transform infrared spectroscopy; TGA/DTA: thermo gravimetric analysis/differential thermal analysis; LUMO: lowest unoccupied molecular orbital; HOMO: highest occupied molecular orbital; PXRD: powder X-ray diffraction (PXRD); PDB: protein data bank; Tyr: tyrosine; His: histidine; Phe: phenylalanine; Asn: asparagine; Ser: serine

ARTICLE HISTORY

Received 13 July 2023
Accepted 30 October 2023

KEYWORDS

CT complex;
spectrophotometric;
pharmacology; molecular
docking; MD simulation

1. Introduction

In instances of partial charge transfer (CT) from an electron source to an electron acceptor molecule, a CT complex is formed by the interaction of these two molecules. The resulting electrostatic attraction plays a pivotal role in stabilizing this complex, albeit being of non-chemical nature, and exhibiting weak binding. The stability of these complexes is predominantly conferred by hydrogen bonding (Khan et al., 2020; 2020; 2021; Oswald et al., 2005). These complexes are notably characterized by their vivid coloration, a feature contingent on the interaction between the Lowest Unoccupied Molecular Orbital (LUMO) of the acceptor and the Highest Occupied Molecular Orbital (HOMO) of the donor (Hamed

et al., 1998). Charge transfer complexes find wide-ranging applications in diverse fields, including surface chemistry (Andrade et al., 2000), photocatalysis (Bhattacharya, 2007), optoelectronics (Coleman et al., 1973; Khan et al., 2011; Sathya et al., 2018; Singh et al., 2015), dendrimers (Jakubiak et al., 2000), biosensors (Kahveci et al., 2017; Li et al., 2013), and chemosensors (Khan & Shakya, 2019; Shakya et al., 2020; Zhang et al., 2017; 2018). Notably, they have gained prominence in biological systems, particularly in antibacterial activities, protein/DNA binding (Khan et al., 2013; 2020; 2022; Khan & Ahmad, 2010), anti-fungal and antimicrobial activities (AlRabiah et al., 2019; Khan et al., 2017), insecticides, antitumor properties, ion transfer across lipophilic membranes (Gutmann et al., 1997; Kidwai et al., 2003), and drug-receptor

binding mechanisms (Adam, 2012; Adam et al., 2019; Islam et al., 2022). The origin of CT complex molecules lies in weak molecular interactions, a concept initially introduced by Mulliken (Mulliken, 1950; Mulliken & Pearson, 1969), extensively investigated later by Foster (Foster, 1969), and further expanded upon by Pauling through the incorporation of hydrogen bonding principles (Pauling, 1960).

8-hydroxyquinoline, an aromatic heterocyclic compound, belongs to a class of compounds characterized by a conjugated system of both π - and n -electrons. Theoretically, this system has the potential to generate two distinct forms of charge-transfer complexes. The charge-transfer complexes of 8-hydroxyquinoline are particularly intriguing due to their ability to shed light on the interaction between p - and n -donor sites with various acceptors. The study of these charge-transfer interactions can significantly contribute to our understanding of a diverse array of chemical and biological phenomena. Moreover, it is well-established that 8-hydroxyquinoline can form hydrogen-bonded structures akin to the base-pairing process observed in RNA and DNA, and it also exists in multiple tautomeric forms (Albert & Phillips, 1956; Forlani et al., 2002; Frank & Katritzky, 1976; Hammes & Lillford, 1970). Extensive research has been conducted on charge transfer complexes of 8-hydroxyquinoline, encompassing its interactions with various acceptors such as 1,4-benzoquinone (Ibrahim, 2011), Citric Acid (Jado et al., 2014), DDQ (Naveen et al., 2016), p -Nitrophenol (Khan et al., 2009), and p -chloranil (Popov & Litvinov, 1979). Additionally, studies have been conducted on the charge transfer complex of Oxalic Acid with Imidazole (Khan et al., 2019) and 2,6-diaminopyridine (Khan et al., 2018). Various medications that demonstrate the capacity to engage in charge-transfer phenomena have been analyzed using Oxalic Acid (OA). The interaction between medicinal chemicals and the electron acceptor culminates in the formation of a highly colored charge-transfer complex that primarily absorbs radiation within the visual spectrum.

The binding of small molecules, known as ligands, to proteins in the bloodstream serves as a valuable means to elucidate the effects and behaviors of these ligands upon entering the circulatory system. The interaction between serum proteins and ligands plays a pivotal role in enhancing protein solubility. Human serum albumin (HSA), the most prevalent protein in blood plasma, constitutes approximately 60% of the total plasma protein. HSA serves as a crucial carrier for drugs, fatty acids, hormones, vitamins, and various other molecules (Khan et al., 2020). Numerous studies have been conducted to explore the binding interactions of ligand molecules with HSA, consistently indicating their propensity to bind to specific sites, namely sites I and II on the HSA protein (Khan et al., 2020).

In the present study, a novel charge transfer complex has been synthesized employing methanol as the solvent in a 1:1 molar ratio between 8-hydroxyquinoline and oxalic acid. The stability and stoichiometry of this charge transfer complex have been evaluated utilizing the straight-line method and the Benesi-Hildebrand method. Furthermore, the complex has been comprehensively characterized through FTIR,

UV-Visible spectroscopy, $^1\text{H-NMR}$, TGA/DTA, and PXRD analyses. Parameters including K_{CT} (stability constant), ϵ (absorptivity coefficient), ΔG° (Gibbs free energy), R_{N} (resonance energy), and other thermodynamic parameters have also been determined. Antibacterial and antifungal activities were explored for the synthesized CT complex and to further explore its drug activity theoretical method (Molecular docking) is used to study the interaction between CT complex and HSA. Additionally, molecular dynamics (MD) simulations of the protein in the presence and absence of the ligand were conducted over a period of 100 ns at 300K, supplemented by MM-PBSA calculations to gain insights into the interactions. Binding free energy calculations further support its pharmaceutical potential.

2. Experimental

2.1. Materials required

Analytical grade of 8-hydroxyquinoline ($\text{C}_9\text{H}_7\text{NO}$) (Merck, purity >99%), and Oxalic acid ($\text{C}_2\text{H}_2\text{O}_4$) (Fisher Scientific, purity > 99%) were used for the synthesis of the complex. Methanol (CHD, purity >99%) Acetone (CHD, purity > 99%), and Distilled water (Laboratory prepared) was used as solvent without doing several more purification.

2.2. Synthesis of charge transfer complex

A concentrated solution of 8-hydroxyquinoline (0.190 gm, 2 mmol) and oxalic acid (0.276 gm, 2 mmol) in methanol was combined to create CT complex (Fig. S1). For two hours, the mixture is stirred at room temperature. As a yellow-colored ppt, the CT complex forms. Using Whatman filter paper, the CT complex is filtered, washed with a small quantity of acetonitrile, and dried under vacuum in a desiccator.

2.3. Standard stock solution preparation

The donor, 8-hydroxyquinoline, was dissolved in a 25 ml volumetric flask using methanol as solvent to dissolve 0.0238 g of it at a 10^{-2} M concentration to create the standard stock solution. By diluting the stock solution in a 25 ml flask, several concentration solutions (1×10^{-4} M to 3.5×10^{-4} M) are created. Oxalic acid was used as the acceptor, and 0.0345 g of OA was dissolved in a 25 ml volumetric flask using methanol and acetone as the solvents to create the standard stock solution at 10^{-2} M. The stock solution of the acceptor was diluted in a 25 ml flask to create a 10^{-4} M solution. Diverse solvents were used in a similar method.

2.4. Instrumentation

2.4.1. FT-IR spectroscopy

Fourier-transfer infrared spectra (FTIR) for 8HQ, OA, and synthesized complex were achieved using a Perkin Elmer spectrometer-version10.03.09 (Kyoto, Japan) through the KBr disc

method. The spectra were collected in the range 400–4000 cm^{-1} .

2.4.2. ¹H-NMR study. ¹H NMR (Proton NMR) experiments were carried out at 298 K in a JEOL JNM ECZ4000S/L1400 MHz spectrometer (Saudi Arabia) and the values are described as chemical shift (δ , ppm). Deuterated chloroform (CDCl_3) was used as a reference solvent.

2.4.3. UV-vis spectra

Using a Perkin Elmer Lambda-365, Serial Number-365K9011403, Operating Range 190–1100 nm, Interface-Tungsten-halogen and Deuterium, Made in Korea was used to study the UV-vis spectra of the 8-hydroxyquinoline, Oxalic acid, and CT complex between 200 and 700 nm at various concentrations. The spectrophotometer has all optical parts and two detectors are included, which have a dimension of 30 × 20 cm. A UV-LED lamp with a continuous light source of 280 nm was passed directly through the samples in order to minimize the loss of light, and the reduced light source was sent to a 1 × 2 fiber coupler.

2.4.4. TGA/DTA analysis

Using an EXSTAR TGA/DTA 6300 modal equipment with a heating rate of 20 °C/min and a nitrogen environment, TGA and DTA of 8-hydroxyquinoline, Oxalic acid, and CT complex were obtained.

2.4.5. Spectrophotometric analysis

To create the stable CT complex, 3 mL of each solution of oxalic acid and 8-hydroxyquinoline were combined in a 1:1 ratio and kept overnight at room temperature. The absorbance of the obtained solution was calculated. Spectrophotometric analysis (Perkin Elmer Lambda-365, Serial Number-365K9011403, Operating Range 190–1100 nm, Interface-Tungsten-halogen and Deuterium, Made in Korea) was used to determine the novel complex's peak wavelength.

2.5. Antimicrobial activities

2.5.1. Antibacterial studies

Through the disc diffusion approach, in-vitro antibacterial tests against *Staphylococcus aureus*, *Escherichia coli*, and *Bacillus subtilis* were created for the CT complex (Cruickshank et al., 1995). Bacterial growth was achieved using nutrient agar. Muller Hinton broth, cultured for 18 h at roughly 37 °C, was utilized in 10 ml of the inoculum solution to standardize the suspension. For the culture to be adjusted to 105 CFU/ml, sterile saline solution was utilized. Different concentrations of solutions, including 0.125, 0.25, 0.5, and 1.0 mg/ml of CT complex, were made, and they significantly inhibited the development of bacterial strains. An agar plate with the required concentration was added, and the zone of inhibition was looked for after 24 h of incubation at 37 °C. The subsequent comparison of the observed effect was made

with gentamicin (a common antibiotic) at a concentration of 1 mg/ml.

2.5.2. Antifungal studies

By using the agar disc diffusion method, the synthesized CT complex was also employed to treat *Aspergillus niger*, *Fusarium oxysporum*, and *Candida albicans* in DMSO. Solutions of CT complex were produced at several concentrations (0.125, 0.25, 0.5, and 1.0 mg/ml) to increase activity. The zone of inhibition (mm) was measured to evaluate the antifungal activity.

2.6. Molecular docking investigation

For docking analysis, HEX 8.0 software (Ritche & Venkataraman, 2010) was employed. Through the online PDB (Protein Data Bank), the structure of the Human Serum Albumin (HSA) with PDB ID 1E78 was discovered. HSA was prepared by removing native ligands, water molecules, and adding polar hydrogen and Kollman charges through Discovery Studio (DS) Visualizer. For docking, Grid: 52x70x86 was used. Chimaera software was used to visualize the docked pose. Overall docking experiment was run on processor (Intel(R) Core(TM) i5-4200U CPU @1.60 GHz 2.10 GHz 2.30 GHz, 64 bit).

2.7. Molecular dynamics simulation (MDS)

Molecular Dynamics Simulation (MDS) plays a pivotal role in investigating how the receptor undergoes structural changes in response to interactions with small compounds over time. Our analysis employed the GROMACS software package, version 2019.2, utilizing the GROMOS96 43a1 force field. CHARMM-GUI facilitated the generation of parameter files and topology, integrating the latest CGenFF version (Vanommeslaeghe et al., 2010; Yu et al., 2012).

The optimal protein-ligand complex selected after molecular docking and unbounded protein was subsequently subjected to MDS investigations. To mimic physiological conditions and achieve system neutrality, we introduced 58 Na^+ and 64 Cl^- ions, equivalent to a physiological salt concentration of 0.15 M, into the solvated system, enclosed within a triclinic box and using the SPC water model (Fig. S2) (Jorgensen et al., 1983). Our simulation adopted periodic boundary conditions under constant pressure (1.0 bar) and temperature (300 K) for a duration of 100 ns, employing a Leap-frog MD integrator during both the NPT and NVT equilibration phases (Allen & Tildesley, 1987; Essmann et al., 1995). Key structural parameters, including hydrogen bonding, gyration radius, solvent-accessible surface area, root mean square fluctuations (RMSF), and root mean square deviation (RMSD), were analyzed using the gmxhbond, gmx gyrate, gmxsasa, gmrxmsf, and gmrxrms tools (Steinbach & Brooks, 1994). Data visualization and plots were generated using Grace Software, with PyMol/VMD assisting in the visualization of the results (DeLano, 2002; Humphrey et al., 1996).

2.8. Binding free energy calculation using MM-PBSA

We employed the molecular mechanics Poisson–Boltzmann surface area (MM-PBSA) method to compute the binding free energies of the protein–ligand complexes. Specifically, we utilized the stable 40 ns trajectories identified through the root mean square deviation (RMSD) analysis. To enhance our understanding of the structure–function relationship, we selected frames at intervals of 200 ps, thus encompassing a diverse range of trajectories and conformational states.

In the single trajectory approach, the following equation represents the full process:

$$\Delta G_{\text{Binding}} = G_{\text{Complex}} - (G_{\text{Receptor}} + G_{\text{Ligand}})$$

$$\Delta G_{\text{MM-PBSA}} = E_{\text{vdW}} + E_{\text{ele}} + G_{\text{polar}} + G_{\text{nonpolar}}$$

The G_{Complex} represents the total MM-PBSA energy of the protein–ligand complex, G_{Receptor} and G_{Ligand} correspond to the total solution free energies of the isolated receptor and ligand, respectively. The $\Delta G_{\text{MM-PBSA}}$ value of the protein–ligand complex was determined from the sum of gas-phase electrostatic energy (E_{ele}), van der Waals (E_{vdW}), polar (G_{polar}), and nonpolar (G_{nonpolar}) components (Lee et al., 2015).

3. Result and discussion

3.1. Comparative studies of FTIR

The FTIR spectra were determined using a frequency range of 4500–500 cm^{-1} . By comparing FTIR spectra of the donor and acceptor, the formation of $[(8\text{-HQ})^+(\text{OX})^-]$ complex was confirmed. As the donor and acceptor bands have been observed at various frequency regions, the strong band's appearance in the newly created CT complex is in various locations, showing the growth of CT complex. The intensity of spectra changes when the symmetry and electrical structure of CT complex creation change. The donor, acceptor, and CT complex FTIR spectra are shown in Fig. S3, and Table 1 lists the observed frequencies. In the FTIR spectra of CT complex, a broad band of $\nu(\text{OH})$ was observed at 3386 cm^{-1} , whereas a broad band of $\nu(\text{OH})$ was observed 3486 cm^{-1} for the free $\text{OH}(\text{COOH})$ of acceptor (Oxalic Acid) and at 3469 cm^{-1} peak appeared for donor (8-hydroxyquinoline). The FTIR spectra for Ar–C–H stretching appeared at 2874 for CT complex, whereas it was observed at 2849 cm^{-1} for donor molecule. It is anticipated that the proton transfer-related stretching vibration $\nu(\text{O}^-\text{H}-\text{N}^+)$, depicted in Scheme 1, will be present at the vibrational peak for the growth of the CT complex, measured at 3051 cm^{-1} . This connection, $\text{O}^-\text{H}-\text{N}^+$, demonstrates that OA and 8HQ formed a brand-new complex. This link, which results from the passage of an electron from the donor nitrogen to the acceptor hydrogen, shows that hydrogen bonds are often weak. The strong peak was seen at 1691 cm^{-1} of $\text{C}=\text{O}$ for oxalic acid, which was absent in the FTIR spectra of CT complex, hence, confirming the formation of CT complex through hydrogen transfer from oxalic acid to 8-hydroxyquinoline. The $\text{C}=\text{C}$ stretching for donor molecule was observed at 1440 cm^{-1} for donor molecule, whereas it appeared at 1467 cm^{-1} for CT complex. The peak

Table 1. FT-IR spectral band assignments (cm^{-1}) of OX and 8-HQ, and CT complex.

Compound	Frequency (cm^{-1})	Assignments	
Oxalic Acid	3486	O-H str	
	1691	$>\text{C}=\text{O}$	
	1630	C-C str	
	1348, 1256	$>\text{C}-\text{O}$	
	1195	O-H bend	
	1087,986	C-O waggassym	
	878,777	O-H torr	
	734,699	C-C wagg	
	8- Hydroxyquinoline	3466	Ar-OH
		2849	Ar-C-H str
2651		$=\text{C}-\text{H}$ out of plane	
1689		$\text{C}=\text{N}$ medium	
1440		$\text{C}=\text{C}$ in ring	
1344		C-N	
1247		C-H in plane bending	
1122		C-H out of plane	
719		O-H torr, C-O wagg	
CT complex		3386	O-H str.
	3051,2935	$\text{ArO}^-\cdots\text{H}-\text{N}^+$	
	2874	Ar-C-H str	
	2772	$=\text{C}-\text{H}$ out of plane	
	1704	$\text{C}=\text{N}$ medium, $>\text{C}=\text{O}$	
	1604	C-C str	
	1541	$\text{C}=\text{C}$ in ring	
	1467	C-N	
	1398	$>\text{C}-\text{O}$ str	
	1292	C-H in plane bending	
1092	C-H out of plane		
750,719	C-C Wagg, O-torr		

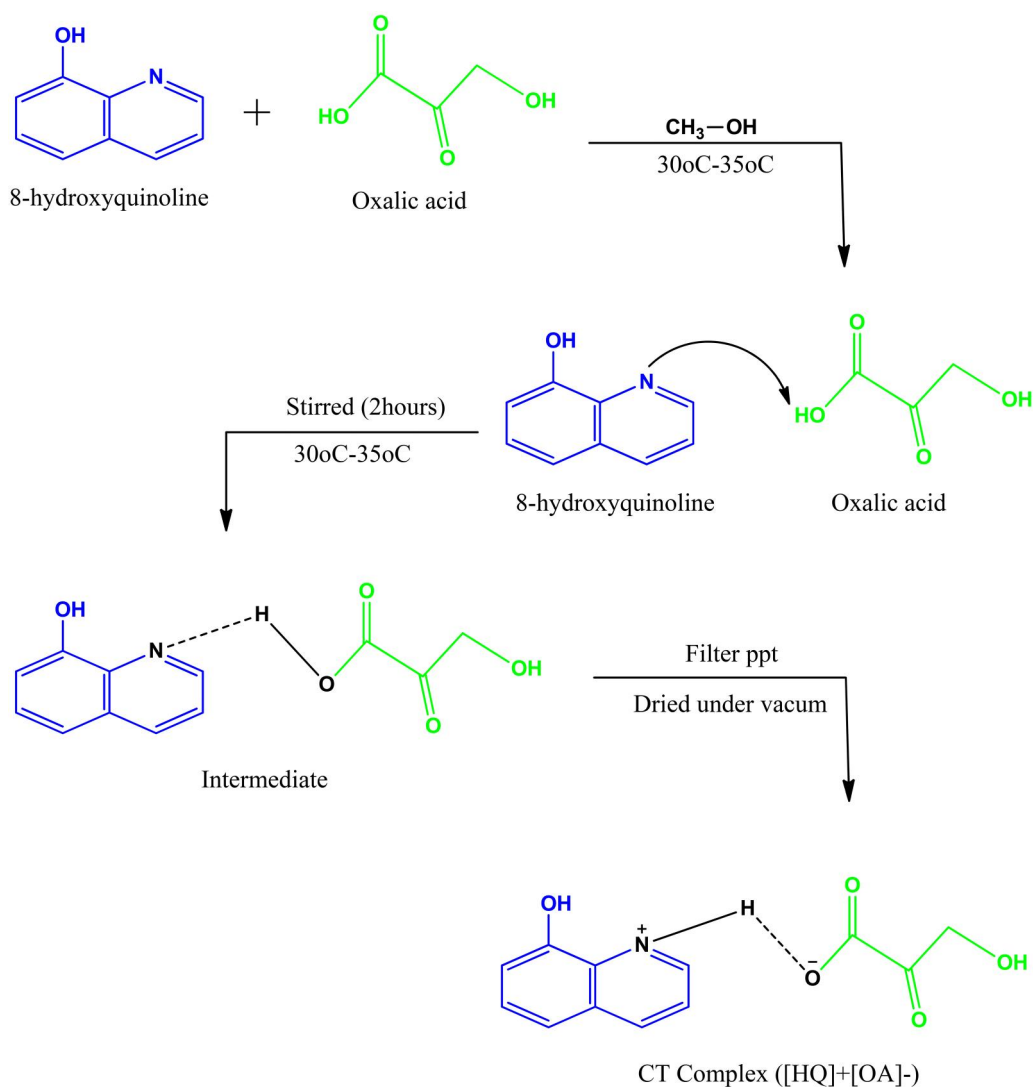
for C–C and C–O was also shifted in the IR spectra of CT complex, indicating the complexation of CT complex.

3.2. CT spectra studies

The UV-absorbance spectra 8-hydroxyquinoline, oxalic acid (1×10^{-4}), and their 1:1 mixture (CT complex) was shown in Figure 1. The λ_{max} value of the synthesized complex was observed at 316 nm, 230 nm in acetone and methanol, respectively. When the donor and acceptor solutions were mixed, a noticeable color change occurred, accompanied by the appearance of a novel charge transfer absorption peak, which was not observed in either the acceptor or donor solutions individually, thus confirming the complexation of CT complex between 8-hydroxyquinoline and oxalic acid. Absorption Band intensity of CT complex was observed is shown in Table 2. The CT spectra of the complex in different solvents are exposed in Figure 1. The Absorption band of CT complex is studied by using The Gaussian function-

$$y = y^0 + \left[\frac{A}{\left(\frac{w}{\sqrt{2}}\right)} \right] \exp \left[-2 \frac{(x - xc)^2}{w^2} \right]$$

Where x = wavelength and y = absorption. Outcomes that were obtained using Gaussian function for all the solutions are shown in Table 4. Wavelength at maximum absorption ($\lambda_{\text{CT}} = xc$) are shown in Table 4. Due to a change in the structure of the CT complex, it can be seen that the λ_{max} of the CT complex is exactly proportional to the polarity of the solvent. The K_{CT} (stability constant) and ϵ_{CT} (molar absorptivity constant), which are given by the following equation, have been obtained using the Benesi Hildebrand equation.



Scheme 1. Charge transfer reaction mechanism between donor and acceptor.

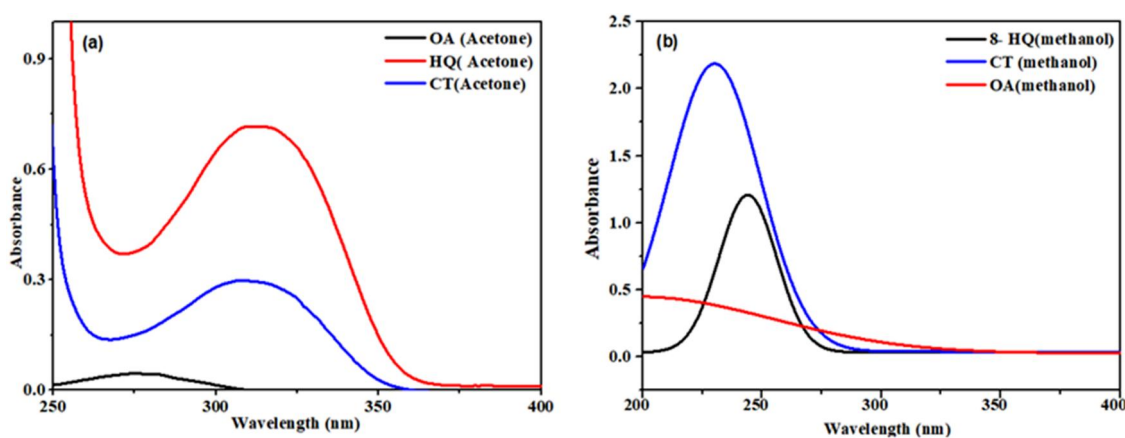


Figure 1. Electronic absorption spectra of acceptor-donor complex ($1 \times 10^{-4} \text{ M} + 1 \times 10^{-4} \text{ M}$) in (a) methanol and (b) acetone, at room temperature.

$$\frac{[A]_0}{A} = \frac{1}{K_{CT}\epsilon_{CT}} \cdot \frac{1}{[D]_0} + \frac{1}{\epsilon_{CT}}$$

Where $[A]_0$ and $[D]_0$, respectively, represent the starting concentrations of oxalic acid and 8-hydroxyquinoline. A is absorbance of CT complex at λ_{CT} in the reference solvent, and the extinction coefficient ϵ_{CT} . The donor

8-hydroxyquinoline concentration was changed between $1 \times 10^{-4} \text{ M}$ and $3 \times 10^{-4} \text{ M}$ in several reaction mixtures, while the acceptor oxalic acid concentration was kept constant at $1 \times 10^{-4} \text{ M}$ in each reaction mixture. Only when the acceptor concentration is greater than the donor concentration or the opposite of it will this equation be true.

Table 2. At room temperature, absorption data for spectrophotometric determination of stoichiometries, absorption maxima (λ_{CT}), formation constants (K_{CT}), and molar extinction coefficients (ϵ_{CT}) of the CT complex.

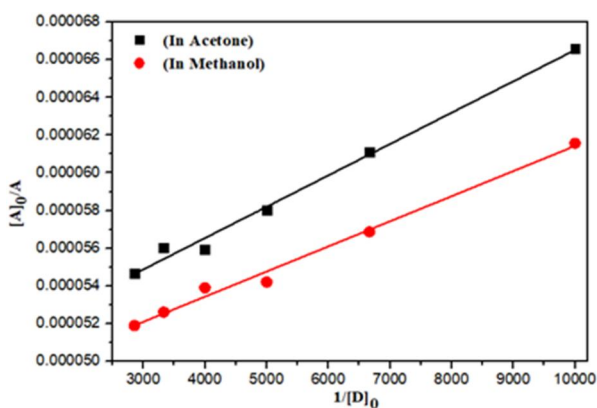
Concentration of donor (M)	Concentration of acceptor (M)	Absorbance at λ_{CT} (nm)	Formation constant (K_{CT})/ mol ⁻¹	Molar extinction coefficient (ϵ_{CT})/ cm ⁻¹ mol ⁻¹
In ethanol	1×10^{-4}	At 230 nm	3.54×10^4	2.17×10^4
1.5×10^{-4}		1.421		
2.0×10^{-4}		1.567		
2.5×10^{-4}		1.623		
3.0×10^{-4}		1.721		
3.5×10^{-4}		1.863		
4.0×10^{-4}		2.012		
In methanol	1×10^{-4}	At 218 nm	3.00×10^4	2.09×10^4
1.5×10^{-4}		1.562		
2.0×10^{-4}		1.691		
2.5×10^{-4}		1.785		
3.0×10^{-4}		1.723		
3.5×10^{-4}		1.856		
4.0×10^{-4}		1.910		

Table 3. Spectral and physical data of the CT complex.

System	Wavelength λ_{CT} (nm)	Ionization potential I_D (eV)	Resonance energy R_N	Energy of Interaction (E_{CT})(eV)	Oscillator strength $f \times 10^{-2}$	Free energy $-\Delta G$ (kJ mol ⁻¹)	Correlation coefficient (r)
Methanol	230	12.49	0.86	0.86	0.096	23.46	0.9785
Acetone	316	11.06	1.23	5.59	0.112	23.13	0.9878

Table 4. Gaussian curve assessment for CT spectra of 8-HQ with OX in various solvents.

System	Area of the curve (A)	Width of the curve (w)	Centre of the curve x_c	y_0
Acetone	187.35257 ± 8.65721	59.0236 ± 2.69421	316.021 ± 1.51804	0.02825 ± 0.01285
Methanol	102.74018 ± 2.52853	38.1432 ± 1.07751	230.14623 ± 0.48455	0.3855 ± 0.01036

**Figure 2.** Benesi-Hildebrand plots of the charge transfer complex of 8-HQ (8-hydroxyquinoline) with OA (acceptor), $[A]_0/a$ vs $1/[D]_0$ in methanol and acetone at room temperature.

By graphing $[A]_0/A$ versus $1/[D]_0$ (Figure 2) in various solvents, the complex's stoichiometry was determined, confirming that the complex was formed in a 1:1 ratio. K_{CT} and ϵ_{CT} were calculated using the slope and intercept on the y-axis of the graph. As the polarity of the solvent lowers, the stability constant rises, indicating the creation of a stable CT complex. The following expression can be used to obtain the energy (E_{CT}) for the CT complex.

$$E_{CT} = 1243.667/\lambda_{CT}nm'$$

where λ_{CT} is the wavelength of complex spectra, the energy drops with rise in the polarity of the solvent.

3.2.1. Ionization potential of donor

Aloisi and Pignataro's empirical equation, which is shown below, was used to calculate the ionization potential (Khan et al., 2022; Lee et al., 2015).

$$I_D(eV) = 5.76 + 1.53 \times 10^{-4} \nu_{CT}$$

I_D stands for ionization potential of the 8HQ molecule, while ν_{CT} stands for wave numbers in cm^{-1} in a different solvent. The calculated ionization potential value is shown in Table 3. The ionization potential of CT complex increases as the polarity of the solvent decreases.

3.2.2. Determination of resonance energy (R_N) and free energy (ΔG°)

As shown below, Briegleb and Czekalla (Aloisi & Pignataro, 1973) have constructed a relation that is utilized to calculate changes in the resonance energy of CT complex.

$$\epsilon_{CT} = 7.7 \times 10^4 / [h\nu_{CT}/R_N] - 3.5$$

where ϵ_{CT} = molar extinction coefficient of CT complex at the highest absorption, which is listed in Table 3 for various solvents and also expresses about the stability of the complex, and R_N is the resonance energy of the complex in the ground state. The frequency of the CT peak is $h\nu_{CT}$. The value of the formation constant can be used to calculate the standard free energy of the CT complex using the equation below.

$$\Delta G = -2.303RT \log K_{CT}'$$

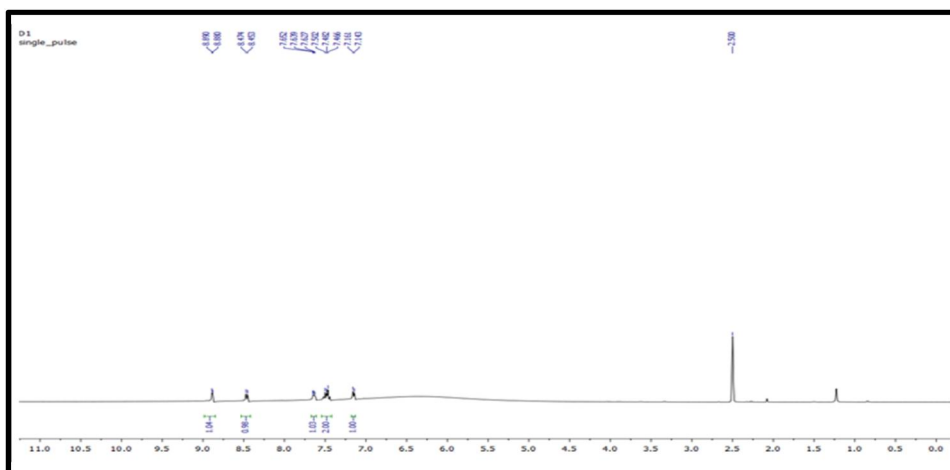


Figure 3. $^1\text{H-NMR}$ spectra of CT complex.

The free energy of the CT complex, the gas constant ($8.314 \text{ Jmol}^{-1}\text{K}^{-1}$), the temperature in Kelvin ($273+^{\circ}\text{C}$), and the formation constant (K_{CT}) of the CT complex in various solvents at room temperature are all listed in Table 3. As the polarity of the solvent increases, so does the value of ΔG .

3.2.3. Determination of oscillator strength and transition dipole moment

The oscillator strength (f) value can be calculated using the following calculation (Briegleb & Czekalla, 1960).

$$f = 4.32 \times 10^{-9} \int \varepsilon_{\text{CT}} \Delta v_{1/2}$$

Where ε_{CT} and $\Delta v_{1/2}$ represent, respectively, the extinction coefficient and band width at half the maximum extinction. The calculated values for the oscillator strength of the CT complex are shown in Table 3. The transition dipole moment and extinction coefficient are connected by the following formula (Kidwai et al., 2003).

$$\mu_{\text{EN}} = 0.0952 [\varepsilon_{\text{CT}} \Delta v_{1/2} / \Delta v]^{1/2}$$

where $\Delta v \approx v$ at ε_{CT} , $\Delta v_{1/2}$ is the half-width of wave number unit. μ_{EN} is the dipole moment, displayed in Table 2.

3.3. $^1\text{H-NMR}$ analysis

^1H NMR spectra of 8HQ, OA and their CT complex were measured in CDCl_3 solvent and are displayed in Figure 3. The phenolic proton of the donor often shows up around 9.72 ppm. Given that a minor peak is seen in the ^1H NMR, it appears to have shifted in the CT complex at 7.68 ppm. The 1:1 ratio of the 8HQ and OA is supported by the ^1H NMR integration of the CT complex. It is abundantly visible from a new peak in the CT complex spectrum that is given a +NH proton at 2.50 ppm and indicates weak protonation of the donor. The spectra of the CT complex contain all of the identified proton peaks from the initial reactant spectrum with a slight upfield shift to lower ppm values. These fluctuations in the (ppm) values of the donor, acceptor, and reaction

product provide strong support for the charge migration from the acceptor (acid) toward the donor (base).

3.4. TGA/DTA analysis

TGA-DTA was used to evaluate the thermal degradation of the synthesized CT complex with a temperature range of 20°C – 800°C and a heating rate of $20^{\circ}\text{C}/\text{min}$. Figure 4 depicts the TGA/DTA curve for the CT complex, acceptor, and donor. According to the DTA plot, oxalic acid exhibits two endothermic peaks at 107°C and 194°C , which correlate to the two stages of weight loss depicted by the TGA curve. The 1.82% weight loss associated with the initial endothermic peak could be the result of the sample losing moisture.

Weight loss of 4.04% corresponds to the second stage of decomposition. In contrast, the 8-hydroxyquinoline DTA curve has two sequential endothermic peaks at 79.29°C and 195°C , which are indicative of the weight loss as depicted by the TGA curve at 5.339%. The thermal decomposition of $[(8\text{-HQ})^+(\text{OX})^-]$ complex occurred in two stages at 135°C and 244°C , with weight losses of 0.243% and 5.631%, respectively, at the decomposition step, according to the TGA/DTA evaluation of the complex at close range (Figure 4). The suggested stoichiometry was supported by the aforesaid data, and the TGA/DTA results showed that heating had an impact on the composition of the CT complex.

3.5. PXRD studies

Powder X-ray spectra were discovered using a P-Analytical XPRT-PRO (Netherlands) diffractometer using the anode materials $\text{Cu K}\alpha_1$, $\text{K}\alpha_2$ and $\text{K}\beta$ radiation at wavelengths 1.540, 1.544, and 1.392, respectively, with angle ranges of 50° – 70° at generator settings 35 mA, 40 kV. Compared to $\text{K}\alpha_2$, $\text{K}\alpha_1$ is more intense and has a somewhat shorter wavelength. The PXRD pattern of the synthesized CT complex, OA, and 8HQ, is shown in Figure 5. For the 8HQ, OA, and $[(8\text{HQ})^+(\text{OA})^-]$ complex, the strongest Bragg's peak was observed at diffraction angles 2θ of 14.68° , 30.31° , and 14.04° , respectively. Due to the sharp peak strength, this proves that the synthesized CT complex is crystalline in nature. The structure of the

recently synthesized complex and the data from the PXRD pattern match up well. For molecules to self-assemble and crystallize, charge transfer between the 8HQ and OA hydroxyl groups is also essential.

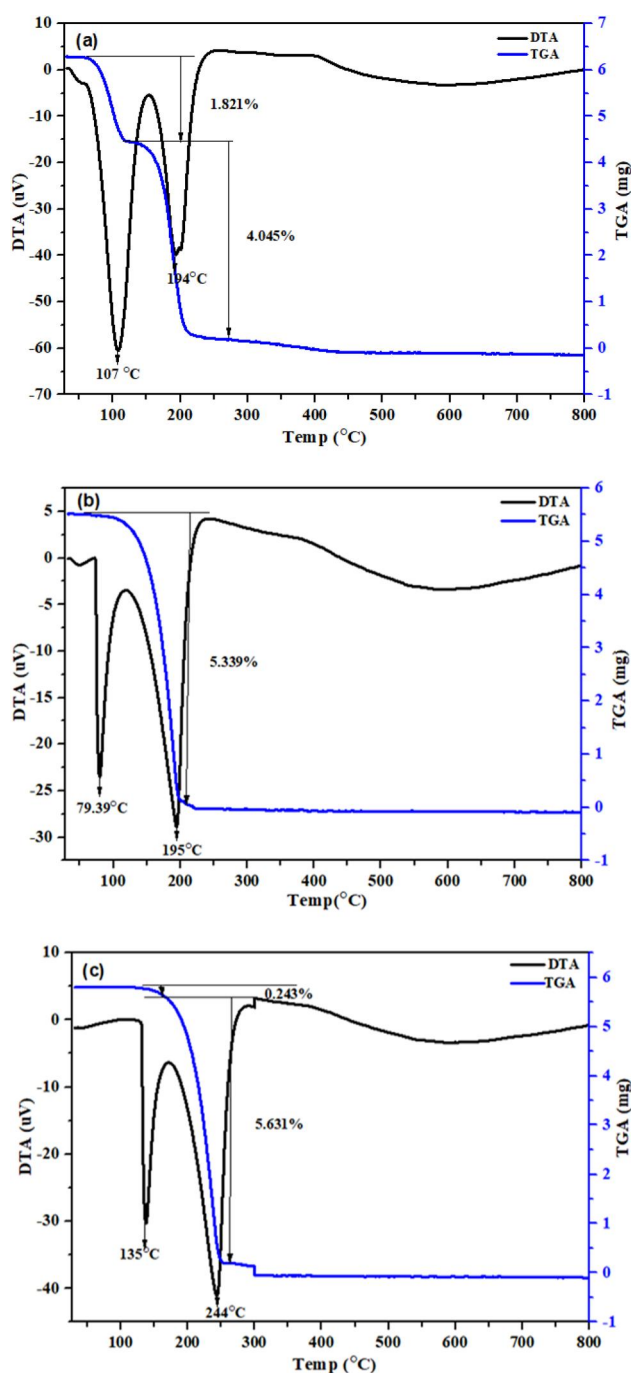


Figure 4. TGA-DTA curves for (a) oxalic acid, (b) 8-hydroxyquinoline, and (c) CT of donor and acceptor.

Table 5. Antibacterial activity of CT- complex at various concentrations.

Sl	Bacterial strain	D1 (10 $\mu\text{g/mL}$)	D2 (20 $\mu\text{g/mL}$)	D3 (40 $\mu\text{g/mL}$)	D4 (80 $\mu\text{g/mL}$)	Gentamicin (80 $\mu\text{g/mL}$)
		Zone of inhibition (mm)				
1.	<i>Escherichia coli</i>	3.2 ± 1.19	7.2 ± 0.98	12.1 ± 1.14	15.8 ± 0.62	35.0 ± 0.62
2.	<i>Bacillus subtilis</i>	9.9 ± 1.34	15.1 ± 1.13	22.2 ± 0.94	28.7 ± 1.25	32.0 ± 1.04
3.	<i>Staphylococcus aureus</i>	10.5 ± 0.92	11.9 ± 0.51	13.18 ± 0.9	19.2 ± 0.72	20.01 ± 0.92

3.6. Antimicrobial investigation

3.6.1. Antibacterial study

The antibacterial activities are investigated using the common medication Gentamicin. For the synthesized CT complex of 8HQ and OA, significant growth inhibition of *Bacterium subtilis*, *Escherichia coli*, and *Staphylococcus aureus* was observed. As shown in Table 5, several CT complex solutions (0.125, 0.25, 0.5, and 1.0 mg/ml) significantly inhibited bacterial growth. The activity against bacterial strain proliferation is depicted in Figure 6. *Staphylococcus aureus* caused the CT complex to exhibit inhibitory zones as well, with *Bacillus subtilis* showing the largest inhibition zone over *Escherichia coli*. Additionally, when CT complex concentrations rise, so do the bacterial growth inhibitory effects. Due to the combined effects of [(8HQ)⁺(OA)⁻] complex penetration into the interior of the cell and cell membrane breakdown, which results in oxidative stress and cell damage, growth inhibition is potentially feasible.

3.6.2. Antifungal study

The antifungal outcomes were compared using the reference medication Nystatin. The 8HQ and OA CT combination demonstrated effective antifungal properties. At a relatively low dosage of 0.25 mg/ml, the CT complex showed audible growth inhibition. A rapid increase in the inhibitory action is shown as the CT complex concentration is raised. *Aspergillus niger*, *Candida albicans*, and *Fusarium oxysporum* all had inhibitory effects in the test complex. Figure 7 and Table 6 in the experimental data gathered demonstrate that CT complex has superior antifungal capabilities to nystatin.

3.7. Molecular docking

The CT complex docked pose with the Human Serum Albumin (HSA) protein was obtained using computational

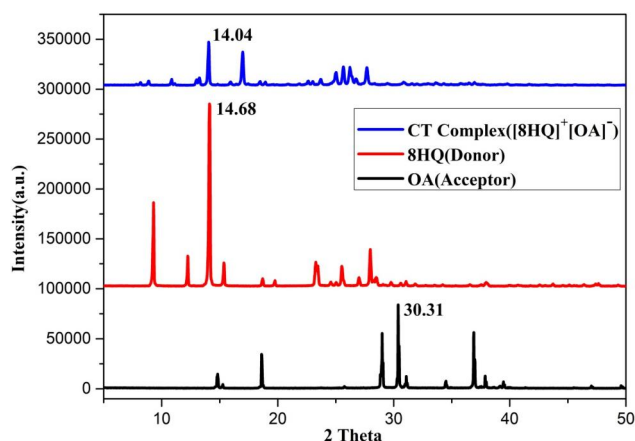


Figure 5. PXRD pattern of the OA (acceptor), 8HQ (donor), and CT complex.

molecular docking. To confirm our experimental findings and provide predictions about the many kinds of interactions between HSA protein-CT complex systems, the potential binding site between the protein and CT complex was investigated. The HSA protein-CT complex system shown in Figure 8 had a free energy of binding (FEB) of -167.04 kJ/mol. The greater interaction between proteins and the production of CT-complex is indicated by the higher value of binding energy. As shown in Figure 8(b), the HSA protein and CT-complex have an estimated binding distance of Tyr 148 = 3.7 Å, His 146 = 2.9 Å, and Phe 149 = 4.8 Å. Tyr and aromatic residue interact to maintain the experimentally determined fluorescence outcome (Devasia et al., 2023; Shakya et al., 2023). Along with Van Der Waals interactions, hydrogen bonds also show a significant role in the binding reaction, as seen between the H of the OXA section of the CT complex and the O of Asn 426 (2.9 Å) and the H of the 8HQ component of the CT Complex and the O of Ser 193 (3.6 Å), Figure 8(a) displays the molecular docking interactions among the protein and CT-complex. The observed experimental results are supported by the potential binding location between the protein and CT complex.

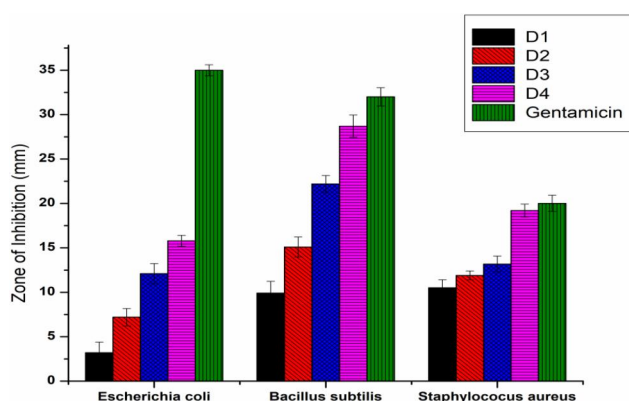


Figure 6. The growth inhibitions against the growth of bacteria at various concentrations are shown.

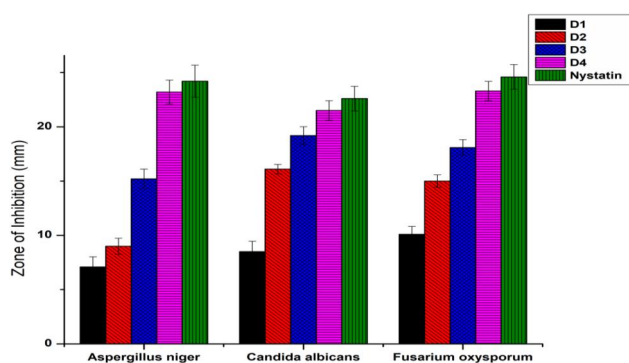


Figure 7. The growth inhibitions against the growth of fungi at various concentrations are shown.

Table 6. Antifungal activity of CT- complex at various concentrations.

	D1 (10 µg/mL)	D2 (20 µg/mL)	D3 (40 µg/mL)	D4 (80 µg/mL)	Nystatin (80 µg/mL)
Fungal strain					
<i>Aspergillusniger</i>	7.1 ± 0.92	9 ± 0.74	15.2 ± 0.9	23.2 ± 1.1	24.2 ± 1.483
<i>Candida albicans</i>	8.5 ± 0.96	16.1 ± 0.44	19.2 ± 0.81	21.5 ± 0.91	22.6 ± 1.140
<i>Fusariumoxysporum</i>	10.1 ± 0.73	15 ± 0.57	18.1 ± 0.72	23.3 ± 0.89	24.6 ± 1.140

Discovery Studio (DS) software was further used to explore the docked complex to display the different surfaces near the ligand (Khan et al., 2013). Aromatic, hydrophobic, interpolated charge and hydrogen bond surfaces at interaction site of CT complex and HSA are represented in Fig. S4. The aromatic face/edge surface (Fig. S4(a), orange/blue = face/edge) has been shown using the docking outputs. The presence of hydrophilicity features of the receptor around the ligand is confirmed by the hydrophobicity surface (Fig. S4(b)). The ionization surface reflected the acidic and basic propensity (Fig. S4(c)), blue colour = basic and red colour = acidic). The hydrogen atom acceptor area is represented with green color and donor area with pink color of the amino acid residues in the hydrogen bond surface, as shown in Fig. S4(d) (Akram et al., 2022; Hassan et al., 2023).

3.8. MSD analysis

The starting structure for the 100ns MD simulation run was the best-docked complex with the highest docking score provided by HEX 8.0 software and unbounded protein. Fig. S1 shows 58 Na^+ and 64 Cl^- ions, equivalent to a physiological salt concentration of 0.15 M , in the solvated system, enclosed within a triclinic box and using the SPC water model. After $\sim 40 \text{ ns}$ and ~ 50 , the unbounded protein and protein-ligand complex acquired stable conformations with an average RMSD value of 2.01 and 2.58 Å, respectively (Figure 9a) (Hasan et al., 2023). This discovery demonstrates that the ligand forms stable protein-ligand combination. The lowest average gyration (Rg) value of ~ 26.67 Å was observed for protein-ligand complex and ~ 27.58 Å for unbounded protein. Rg for the protein-ligand combination dropped with time, indicating that the structure becomes more compact. (Figure 9b). Grid-search on $14 \times 14 \times 17$ grid, $\text{rcut} = 0.35$, revealed the number of hydrogen bond interactions between ligand and protein, which were plotted against time (Figure 10a). On calculating hydrogen bonds between ligand and proteins, 689 donors and 1548 acceptors were found. The average number of hydrogen bonds per timeframe was observed to be 2.7494 out of 601709 possible. As shown in Figure 10(b), the SASA (solvent accessible surface area) values decrease on binding of ligand to protein, showing that the protein structure has changed and that the pocket size has shrunk due to increasing hydrophobicity (Alsanie et al., 2022).

3.9. Binding free energy calculation using MM-PBSA

The binding free energy of the protein-ligand complex was assessed by conducting a 40 ns molecular dynamics (MD) simulation to validate the inhibitor's affinity, as initially predicted through docking simulations. We employed the MM-PBSA method to calculate the cumulative nonpolar, polar,

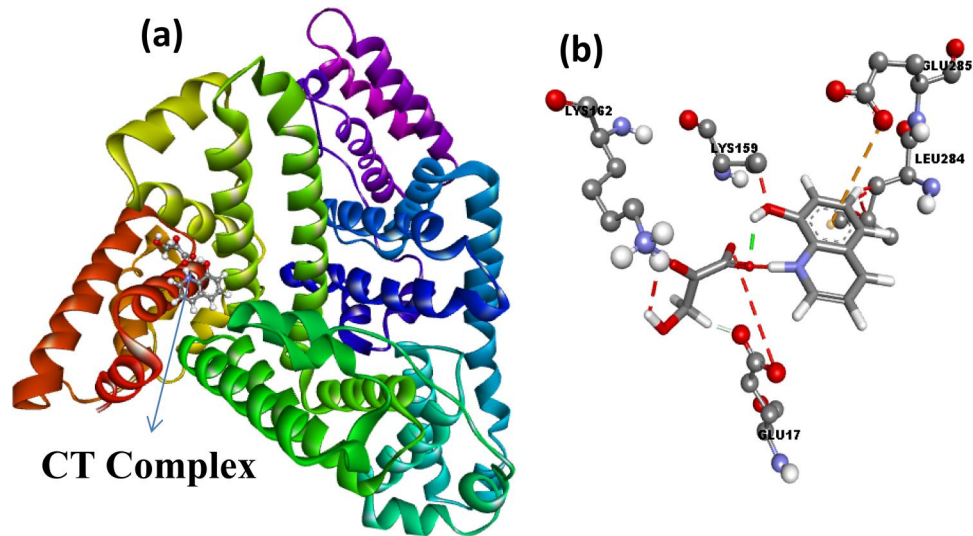


Figure 8. (a) Docking pose showing interaction between CT complex and HSA (b) the 2D view showing different types of bonds between CT complex and HSA.

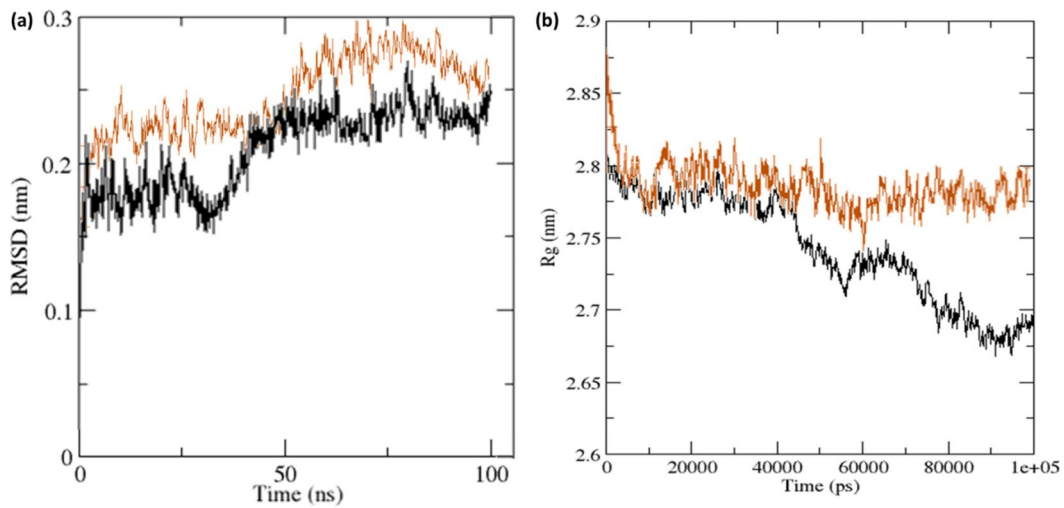


Figure 9. (a) The root mean square deviation (RMSD) during 100 ns MDS run for unbound protein (brown) and protein-ligand complex (black); (b) radius of gyration (R_g) for unbound protein (brown) and protein-ligand complex (black) during 100 ns simulation time.

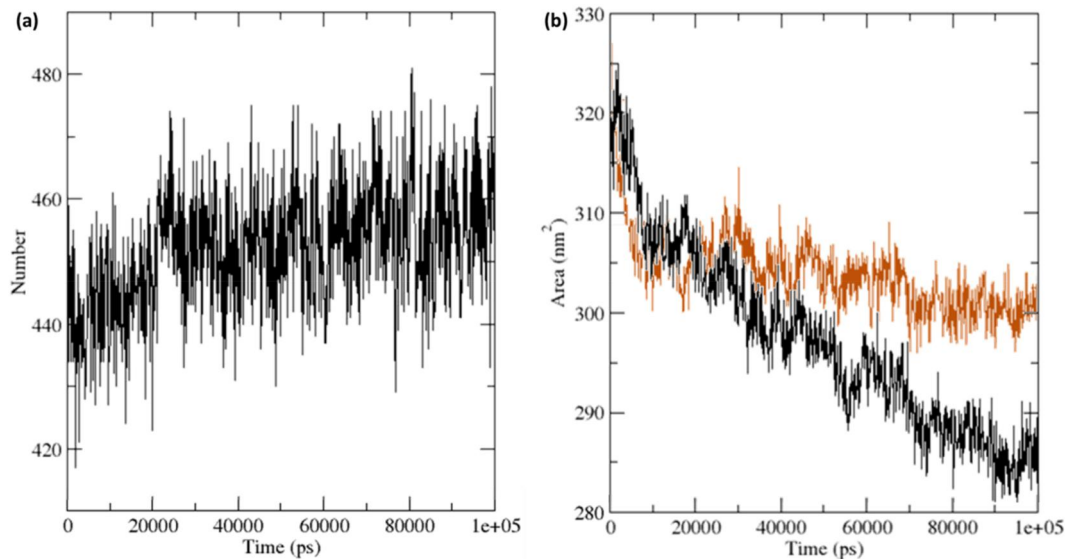


Figure 10. (a) Number of average hydrogen bonding interactions between protein and ligand during 100 ns simulation time and (b) SASA analysis for unbound protein (brown) and protein-ligand complex (black) during 100 ns simulation time.

Table 7. Binding free energies (\pm standard deviations) from MM-PBSA calculations for protein-ligand complex.

	Protein-ligand complex energies in (kJ/mol)
Binding energy (Total)	-86.194 ± 1.843
Van der Waals energy (E_{vdw})	-43.501 ± 4.043
Electrostatic energy (E_{elec})	-190.227 ± 2.983
Nonpolar solvation energy ($G_{nonpolar}$)	-61.006 ± 5.187
Polar solvation energy (G_{polar})	208.840 ± 2.999

and non-bonded interaction energies; encompassing electrostatic and van der Waals forces, for both complexes (Table 7). The computed binding energy for the protein-ligand complex was determined to be -86.194 kJ/mol. Notably, these MD simulation-derived binding energies corroborate the favorable binding affinity predicted by the docking studies. Specifically, the van der Waals energy of the protein-ligand complex was -43.501 kJ/mol, with the electrostatic energy exhibiting a moderate contribution. The solvent-accessible surface area (SASA) energy and polar solvation effects moderately influenced the overall binding energy. In summary, these results collectively suggest the stability of the protein-ligand complex (Alamri et al., 2022; Hasan et al., 2023).

4. Conclusion

This study presents a comprehensive investigation into the formation and characterization of a novel charge transfer complex between 8-hydroxyquinoline (8HQ) and oxalic acid (OA) through N^+H-O^- type of bonding between them. The complex formation was confirmed through various spectroscopic techniques, including FT-IR, UV-visible, and 1H -NMR. The stoichiometry of the complex was determined to be 1:1. TGA/DTA analysis revealed the thermal behavior of the complex, confirming its stability. PXRD studies demonstrated the crystalline nature of the complex, supporting the CT interactions between the donor and acceptor molecules. Antimicrobial studies indicated significant inhibitory effects of the complex against both bacterial and fungal strains, highlighting its potential in pharmaceutical applications. Molecular docking analysis with Human Serum Albumin (HSA) provided insights into the potential interactions between the complex and a relevant protein target. Molecular dynamics simulations further supported the stability of the protein-ligand complex over a 100 ns period. Lastly, binding free energy calculations using MM-PBSA reaffirmed the favorable binding affinity observed in the docking studies, indicating the potential of the complex as a promising candidate for further development in pharmaceutical applications. Overall, this study not only contributes to the understanding of CT complexes but also underscores the potential of the synthesized complex for various applications in the fields of pharmaceuticals and materials science. Molecular interactions with HSA demonstrate strong affinity, indicating potential drug-receptor interactions. Furthermore, *in-vivo* assessments are essential for a comprehensive understanding of the therapeutic potential of the CT complex and for exploring additional biological activities beyond its antibacterial and antifungal properties.

Acknowledgements

The authors would like to convey their gratitude to the Department of Chemistry, Faculty of Science, University of Tabuk, Saudi Arabia, for its enthusiastic support of their present endeavors.

Disclosure statement

No potential conflict of interest was reported by the authors.

Funding

The author(s) reported there is no funding associated with the work featured in this article.

ORCID

Sonam Shakya  <http://orcid.org/0000-0002-3581-8545>

References

- Aloisi, G. G., & Pignataro, S. (1973). Molecular complexes of substituted thiophens with r and p acceptors. Charge transfer spectra and ionization potentials of the donors. *Journal of the Chemical Society, Faraday Transactions 1: Physical Chemistry in Condensed Phases*, 69(0), 534–539. <https://doi.org/10.1039/f19736900534>
- Hassan, M. I., Umair, M., Mathur, Y., Mohammad, T., Khan, A., Sulaimani, M. N., ... Islam, A. (2023). Molecular dynamics simulation to study thermal unfolding in proteins. In *Protein folding dynamics and stability: Experimental and computational methods* (pp. 221–249). Springer Nature Singapore.
- Hasan, A. H., Shakya, S., Hussain, F. H. S., Murugesan, S., Chander, S., Pratama, M. R. F., Jamil, S., Das, B., Biswas, S., & Jamalis, J. (2023). Design, synthesis, anti-acetylcholinesterase evaluation and molecular modelling studies of novel coumarin-chalcone hybrids. *Journal of Biomolecular Structure & Dynamics*, 1–13. <https://doi.org/10.1080/07391102.2022.2162583>
- Pauling, L. (1960). *The nature of the chemical bond*. Cornell University Press.
- Adam, A. M. (2012). Synthesis, spectroscopic, thermal and antimicrobial investigations of charge transfer complexes formed from the drug procaine hydrochloride with quinol, picric acid and TCNQ. *J MolStruct*, 1030, 26–39. <https://doi.org/10.1016/j.molstruc.2012.07.017>
- Adam, A. M. A., Eldaroti, H. H., Hegab, M. S., Refat, M. S., Al-Humaidi, J. Y., & Saad, H. A. (2019). Measurements and correlations in solution state for charge transfer products caused from the 1: 2 complexation of TCNE acceptor with several important drugs. *Spectrochimica Acta. Part A, Molecular and Biomolecular Spectroscopy*, 211, 166–177. <https://doi.org/10.1016/j.saa.2018.12.008>
- Akram, Mohd., Lal, Hira, Shakya, Sonam, Varshney, Rohit, Kabir-ud-Din, (2022). Molecular engineering of complexation between RNA and biodegradable cationic Gemini surfactants: Role of the hydrophobic chain length. *Molecular Systems Design & Engineering*, 7(5), 487–506. <https://doi.org/10.1039/D1ME00147G>
- Alamri, A. S., Alhomrani, M., Alsanie, W. F., Alyami, H., Shakya, S., Habeeballah, H., Abdulaziz, O., Alamri, A., Alkhatabi, H. A., Felimban, R. I., Alhabeeb, A. A., Refat, M. S., & Gaber, A. (2022). Spectroscopic and molecular docking analysis of π -acceptor complexes with the drug barbitol. *Applied Sciences*, 12(19), 10130. <https://doi.org/10.3390/app121910130>
- Albert, A., & Phillips, J. N. (1956). 264. Ionization constants of heterocyclic substances. Part II. Hydroxy-derivatives of nitrogenous six-membered ring-compounds. *Journal of the Chemical Society (Resumed)*, 1294–1304. <https://doi.org/10.1039/jr9560001294>
- Allen, M. P., & Tildesley, D. J. (1987). *computer simulations of liquids*. Oxford.

- AlRabiah, H., Abdel-Aziz, H. A., & Mostafa, G. A. (2019). Charge transfer complexes of brucine with chloranilic acid, 2, 3-dichloro-5, 6-dicyano-1, 4-benzoquinone and tetracyanoquinodimethane: Synthesis, spectroscopic characterization and antimicrobial activity. *Journal of Molecular Liquids*, 286, 110754. <https://doi.org/10.1016/j.molliq.2019.04.031>
- Alsanie, W. F., Alamri, A. S., Alyami, H., Alhomrani, M., Shakya, S., Habeeballah, H., Alkhatibi, H. A., Felimban, R. I., Alzahrani, A. S., Alhabeeb, A. A., Raafat, B. M., Refat, M. S., & Gaber, A. (2022). Increasing the efficacy of seproxetine as an antidepressant using charge-transfer complexes. *Molecules (Basel, Switzerland)*, 27(10), 3290. <https://doi.org/10.3390/molecules27103290>
- Andrade, S. M., Costa, S. M., & Pansu, R. (2000). Structural changes in W/O Triton X-100/cyclohexane-hexanol/water microemulsions probed by a fluorescent drug Piroxicam. *Journal of Colloid and Interface Science*, 226(2), 260–268. <https://doi.org/10.1006/jcis.2000.6821>
- Bhattacharya, S. (2007). Ab initio and TD-DFT investigations on charge transfer transition for the o-chloranil/aniline complex in gas phase. *Chemical Physics Letters*, 446(1–3), 199–205. <https://doi.org/10.1016/j.cplett.2007.08.041>
- Briegleb, G., & Czekalla, J. (1960). Elektronenüberführung durch Lichtabsorption und -emission in Elektronen-Donator-Acceptor-Komplexen. *Angewandte Chemie*, 72(12), 401–413. <https://doi.org/10.1002/ange.19600721203>
- Coleman, L. B., Cohen, M. J., Sandman, D. J., Yamagishi, F. G., Garito, A. F., & Heeger, A. J. (1973). Superconducting fluctuations and the Peierls instability in an organic solid. *J Solid State Commun*, 12(11), 1125–1132. [https://doi.org/10.1016/0038-1098\(73\)90127-0](https://doi.org/10.1016/0038-1098(73)90127-0)
- Cruickshank, R., Duguid, J. P., Marmion, B. P., & Swain, R. H. A. (1995). *Awain medicinal microbiology* (12th ed.). Churchill Livingstone London, 196.
- DeLano, W. L. (2002). PyMOL.DeLano Scientific.
- Devasia, J., Chinnam, S., Khatana, K., Shakya, S., Joy, F., Rudrapal, M., & Nizam, A. (2023). Synthesis, DFT and in silico anti-COVID evaluation of novel tetrazole analogues. *Polycyclic Aromatic Compounds*, 43(3), 1941–1956. <https://doi.org/10.1080/10406638.2022.2036778>
- Essmann, U., Perera, L., Berkowitz, M. L., Darden, T., Lee, H., & Pedersen, L. G. (1995). A smooth particle Mesh Ewald method. *The Journal of Chemical Physics*, 103(19), 8577–8593. <https://doi.org/10.1063/1.470117>
- Forlani, L., Cristoni, G., Boga, C., Todesco, P. E., Vecchio, E. D., Selva, S., & Monari, M. (2002). Reinvestigation of the tautomerism of some substituted 2-hydroxypyridines. *Arkivoc*, 2002(11), 198–215. <https://doi.org/10.3998/ark.5550190.0003.b18>
- Foster, R. (1969). *Charge transfer complexes*. Academic Press.
- Frank, J., & Katritzky, A. R. (1976). Tautomeric pyridines. Part XV. Pyridone-hydroxypyridine equilibria in solvents of differing polarity. *J. Chem. Soc. Perkin Trans*, 2(12), 1428–1431. <https://doi.org/10.1039/P29760001428>
- Gutmann, F., Johnson, C., & Keyzer, H. (1997). *Molnar J charge transfer complexes in biochemistry systems*. Marcel Dekker Inc.
- Hamed, M. M. A., Abdel-Hamid, M. I., & Mahmoud, M. R. (1998). Molecular complexes of some N arylthiocarbamates with π -electron acceptors. *Monatshefte Für Chemie / Chemical Monthly*, 129(2), 121–127. <https://doi.org/10.1007/PL00010148>
- Hammes, G. G., & Lillford, P. J. (1970). Kinetic and equilibrium study of the hydrogen bond dimerization of 2-pyridone in hydrogen bonding solvents. *Journal of the American Chemical Society*, 92(26), 7578–7585. <https://doi.org/10.1021/ja00729a012>
- Hasan, A. H., Yusof, F. S. M., Kamarudin, N. A., Murugesan, S., Shakya, S., & Jamal, J. (2023). Synthesis, anti-acetylcholinesterase evaluation, molecular docking and molecular dynamics simulation of novel Psoralen derivatives. *Current Organic Synthesis*, <https://doi.org/10.2174/1570179420666230328121554>
- Humphrey, W., Dalke, A., & Schulten, K. (1996). VMD: Visual molecular dynamics. *Journal of Molecular Graphics*, 14(1), 33–38. [https://doi.org/10.1016/0263-7855\(96\)00018-5](https://doi.org/10.1016/0263-7855(96)00018-5)
- Ibrahim, A. A. (2011). Spectrophotometric studies of charge transfer complex of 8-hydroxyquinoline with 1, 4-benzoquinone. *Afr. J. Pure Appl. Chem*, 5(16), 507–514.
- Islam, M., Khan, I. M., Shakya, S., & Alam, N. (2022). Design, synthesis, characterizing and DFT calculations of a binary CT complex co-crystal of bioactive moieties in different polar solvents to investigate its pharmacological activity. *Journal of Biomolecular Structure & Dynamics*, 1–17. <https://doi.org/10.1080/07391102.2022.2158937>
- Jado, D., Siraj, K., & Meka, N. (2014). Electron donor-acceptor interaction of 8-hydroxyquinoline with citric acid in different solvents: spectroscopic studies. *Journal of Applied Chemistry*, 2014, 1–7. <https://doi.org/10.1155/2014/484361>
- Jakubiak, R., Bao, Z., & Rothberg, L. (2000). Dendritic sidegroups as three-dimensional barriers to aggregation quenching of conjugated polymer fluorescence. *Synthetic Metals*, 114(1), 61–64. [https://doi.org/10.1016/S0379-6779\(00\)00225-3](https://doi.org/10.1016/S0379-6779(00)00225-3)
- Jorgensen, W. L., Chandrasekhar, J., Madura, J. D., Impey, R. W., & Klein, M. L. (1983). Comparison of simple potential functions for simulating liquid water. *The Journal of Chemical Physics*, 79(2), 926–935. <https://doi.org/10.1063/1.445869>
- Kahveci, Z., Martínez-Tomé, M. J., Mallavia, R., & Mateo, C. R. (2017). Fluorescent biosensor for phosphate determination based on immobilized polyfluorene-liposomal nanoparticles coupled with alkaline phosphatase. *ACS Applied Materials & Interfaces*, 9(1), 136–144. <https://doi.org/10.1021/acsami.6b12434>
- Khan, I. M., & Ahmad, A. (2010). Synthesis, characterization, structural, spectrophotometric and antimicrobial activity of charge transfer complex of p-phenylenediamine with 3, 5 dinitrosalicylic acid. *J Mol Struct*, 975(1-3), 381–388. <https://doi.org/10.1016/j.molstruc.2010.05.014>
- Khan, I. M., Ahmad, A., Miyan, L., Ahmad, M., & Aziz, N. (2017). Synthesis of charge transfer complex of chloranilic acid as acceptor with p-nitroaniline as donor: Crystallographic, UV visible spectrophotometric and antimicrobial studies. *J Mol Struct*, 1141, 687–697.
- Khan, I. M., Ahmad, A., & Ullah, M. F. (2011). Synthesis, crystal structure, antimicrobial activity and DNA-binding of hydrogenbonded proton-transfer complex of 2, 6-diaminopyridine with picric acid. *Journal of Photochemistry and Photobiology. B, Biology*, 103(1), 42–49. <https://doi.org/10.1016/j.jphotobiol.2011.01.010>
- Khan, I. M., Ahmad, A., & Ullah, M. F. (2013). Synthesis, spectroscopic investigations, antimicrobial and DNA binding studies of a new charge transfer complex of o-phenylenediamine with 3, 5 dinitrosalicylic acid. *Spectrochimica Acta. Part A, Molecular and Biomolecular Spectroscopy*, 102, 82–87. <https://doi.org/10.1016/j.saa.2012.10.027>
- Khan, I. M., Alam, K., Afshan, M., Shakya, S., & Islam, M. (2020). Thermodynamic and structural studies of newly prepared CT complex between pyrazole as donor and salicylic acid as acceptor at various temperatures in ethanol. *Journal of Molecular Structure*, 1206, 127758. <https://doi.org/10.1016/j.molstruc.2020.127758>
- Khan, I. M., Alam, K., Alam, M. J., & Ahmad, M. (2019). Spectrophotometric and photocatalytic studies of H-bonded charge transfer complex of oxalic acid with imidazole: single crystal XRD, experimental and DFT/TD-DFT studies. *New Journal of Chemistry*, 43(23), 9039–9051. <https://doi.org/10.1039/C9NJ00332K>
- Khan, I. M., Islam, M., Shakya, S., Alam, K., Alam, N., & Shahid, M. (2020). Synthesis, characterization, antimicrobial and DNA binding properties of an organic charge transfer complex obtained from pyrazole and chloranilic acid. *Bioorganic Chemistry*, 99, 103779. <https://doi.org/10.1016/j.bioorg.2020.103779>
- Khan, I. M., Islam, M., Shakya, S., Alam, N., Imtiaz, S., & Islam, M. (2022). Synthesis, spectroscopic characterization, antimicrobial activity, molecular docking and DFT studies of proton transfer (H-bonded) complex of 8-aminoquinoline (donor) with chloranilic acid (acceptor). *Journal of Biomolecular Structure & Dynamics*, 40(22), 12194–12208. <https://doi.org/10.1080/07391102.2021.1969280>
- Khan, I. M., & Shakya, S. (2019). Exploring colorimetric real-time sensing behavior of a newly designed CT complex toward nitrobenzene and Co²⁺: Spectrophotometric, DFT/TD-DFT, and mechanistic insights. *ACS Omega*, 4(6), 9983–9995. <https://doi.org/10.1021/acsomega.9b01314>
- Khan, I. M., Shakya, S., Akhtar, R., Alam, K., Islam, M., & Alam, N. (2020). Exploring interaction dynamics of designed organic cocrystal charge transfer complex of 2 hydroxypyridine and oxalic acid with human serum albumin: Single crystal, spectrophotometric, theoretical and

- antimicrobial studies. *Bioorganic Chemistry*, 100, 103872. <https://doi.org/10.1016/j.bioorg.2020.103872>
- Khan, I. M., Shakya, S., Islam, M., Khan, S., & Najnin, H. (2021). Synthesis and spectrophotometric studies of CT complex between 1, 2-dimethylimidazole and picric acid in different polar solvents: Exploring antimicrobial activities and molecular (DNA) docking. *Physics and Chemistry of Liquids*, 59(5), 753–769. <https://doi.org/10.1080/00319104.2020.1810250>
- Khan, I. M., Shakya, S., & Singh, N. (2018). Preparation, single-crystal investigation and spectrophotometric studies of proton transfer complex of 2, 6-diaminopyridine with oxalic acid in various polar solvents. *Journal of Molecular Liquids*, 250, 150–161. <https://doi.org/10.1016/j.molliq.2017.11.150>
- Khan, I. M., Singh, N., & Ahmad, A. (2009). Spectroscopic studies of multiple charge transfer complexes of 8-hydroxyquinoline with π acceptor p-nitrophenol in different solvents at room temperature. *Canadian Journal of Analytical Sciences and Spectroscopy*, 54(1), 31–37.
- Khan, T., Waseem, R., Zehra, Z., Aiman, A., Bhardwaj, P., Ansari, J., ... Islam, A. (2022). Mitochondrial dysfunction: Pathophysiology and mitochondria-targeted drug delivery approaches. *Pharmaceutics*, 14(12), 2657. <https://doi.org/10.3389/fphar.2015.00011>
- Kidwai, M., Saxena, S., Rastogi, S., & Venkataramanan, R. (2003). Pyrimidines as anti-infective agents. *Current Medicinal Chemistry -Anti-Infective Agents*, 2(4), 269–286. <https://doi.org/10.2174/1568012033483015>
- Lee, H.-K., Zhang, L., Smith, M. D., Walewska, A., Vellore, N. A., Baron, R., McIntosh, J. M., White, H. S., Olivera, B. M., & Bulaj, G. (2015). A marine analgesic peptide, contulakin-G, and neurotensin are distinct agonists for neurotensin receptors: Uncovering structural determinants of desensitization properties. *Frontiers in Pharmacology*, 6, 11. <https://doi.org/10.3389/fphar.2015.00011>
- Li, M., Zhou, X., Ding, W., Guo, S., & Wu, N. (2013). Fluorescent aptamer-functionalized graphene oxide biosensor for label-free detection of mercury (II). *Biosensors & Bioelectronics*, 41, 889–893. <https://doi.org/10.1016/j.bios.2012.09.060>
- Mulliken, R. S. (1950). Structures of complexes formed by halogen molecules with aromatic and with oxygenated solvents 1. *Journal of the American Chemical Society*, 72(1), 600–608. <https://doi.org/10.1021/ja01157a151>
- Mulliken, R. S., & Pearson, W. B. (1969). *Molecular complexes*. Wiley Publishers.
- Naveen, B., Arunapriya, L., & Parthasarathy, T. (2016). "Charge transfer interaction of 8-hydroxyquinoline with DDQ: Spectrophotometric, thermodynamic and molecular modeling studies."
- Oswald, I. D., Samuel Motherwell, W. D., & Parsons, S. (2005). Formation of quinol co crystals with hydrogen-bond acceptors. *Acta Crystallographica. Section B, Structural Science*, 61(Pt 1), 46–57. <https://doi.org/10.1107/S0108768104028605>
- Popov, Y. P., & Litvinov, V. P. (1979). Molecular complexes of 8-hydroxyquinoline transition-metal chelates with p-chloranil. *Bulletin of the Academy of Sciences of the USSR Division of Chemical Science*, 28(1), 54–57. <https://doi.org/10.1007/BF00925397>
- Ritche, D. W., & Venkataraman, V. (2010). Ultra-fast FFT protein docking on graphics processors. *Bioinformatics*, 26, 2398.
- Sathya, K., Dhamodharan, P., & Dhandapani, M. (2018). Structural characterization and DFT study of a new optical crystal: 2-amino-3-methylpyridinium-3, 5-dinitrobenzoate. *Optics & Laser Technology*, 101, 328–340. <https://doi.org/10.1016/j.optlastec.2017.11.027>
- Shakya, S., Khan, I. M., & Ahmad, M. (2020). Charge transfer complex based real-time colorimetric chemosensor for rapid recognition of dinitrobenzene and discriminative detection of Fe²⁺ ions in aqueous media and human hemoglobin. *J PhotochemPhotobio A*, 392, 112402. <https://doi.org/10.1016/j.jphotochem.2020.112402>
- Shakya, S., Khan, I. M., Shakya, B., Siddique, Y. H., Varshney, H., & Jyoti, S. (2023). Protective effect of the newly synthesized and characterized charge transfer (CT) complex against are coline induced toxicity in third-instar larvae of transgenic *Drosophila melanogaster* (hsp70-lacZ) Bg 9: Experimental and theoretical mechanistic insights. *Journal of Materials Chemistry B*, 11(6), 1262–1278. <https://doi.org/10.1039/D2TB02362H>
- Singh, N., Khan, I. M., & Ahmad, A. (2015). Synthesis and spectrophotometric studies of charge transfer complexes of benzamide with picric acid in different polar solvents. *Research on Chemical Intermediates*, 41(3), 1843–1861. <https://doi.org/10.1007/s11164-013-1474-8>
- Steinbach, P. J., & Brooks, B. R. (1994). New spherical-cutoff methods for long-range forces in macromolecular simulation. *Journal of Computational Chemistry*, 15(7), 667–683. <https://doi.org/10.1002/jcc.540150702>
- Vanommeslaeghe, K., Hatcher, E., Acharya, C., Kundu, S., Zhong, S., Shim, J., Darian, E., Guvench, O., Lopes, P., Vorobyov, I., & Mackerell, A. D. Jr. (2010). CHARMM general force field: A force field for drug-like molecules compatible with the CHARMM all-atom additive biological force fields. *Journal of Computational Chemistry*, 31(4), 671–690. <https://doi.org/10.1002/jcc.21367>
- Yu, W., He, X., Vanommeslaeghe, K., & MacKerell, A. D. Jr. (2012). Extension of the CHARMM General Force Field to sulfonylcontaining compounds and its utility in biomolecular simulations. *Journal of Computational Chemistry*, 33(31), 2451–2468. <https://doi.org/10.1002/jcc.23067>
- Zhang, J., Jin, J., Xu, H., Zhang, Q., & Huang, W. (2018). Recent progress on organic donor–acceptor complexes as active elements in organic field-effect transistors. *Journal of Materials Chemistry C*, 6(14), 3485–3498. <https://doi.org/10.1039/C7TC04389A>
- Zhang, J., Xu, W., Sheng, P., Zhao, G., & Zhu, D. (2017). Organic donor–acceptor complexes as novel organic semiconductors. *Accounts of Chemical Research*, 50(7), 1654–1662. <https://doi.org/10.1021/acs.accounts.7b00124>